Research Square

Preprints are preliminary reports that have not undergone peer review.
They should not be considered conclusive, used to inform clinical practice,
or referenced by the media as validated information.

Fisetin-Preconditioned ADSCs for Intranasal Therapy of Traumatic Brain Injury: Nrf2/HO-1-Associated Stress Resistance and Microenvironment Remodeling

Jianfei Wu
Southwest Medical University
Yu Liu
Southwest Medical University
Yuanyuan Zeng
Southwest Medical University
Youguo Tan
Southwest Medical University
Bo Liu
liubo25110163.com
Southwest Medical University

Research Article

Keywords: Traumatic brain injury. ADSCs. Fisetin. Microglia. Nrf2, HO-1

Posted Date: November 18th, 2026

DOI: https://doi.org/10.21203/rs.3.rs-11616200/v1

License: This work is licensed under a Creative Commons Attribution 4.0 International License.
Read Full License

Additional Declarations: No competing interests reported.

Fisetin-Preconditioned ADSCs for Intranasal Therapy of Traumatic Brain Injury: Nrf2/HO-1-Associated Stress Resistance and Microenvironment Remodeling

Jianfei Wu[1,2,3]. Yu Liu[1,2,3]. Yuanyuan Zeng[1,2]. Youguo Tan[1,2,3]. Bo Liu[1,2,3].

[1] School of Mental Health, Southwest Medical University, Zigong 643021, Sichuan, China

[2] Department of Psychiatry, Zigong Mental Health Center, Zigong 643021, Sichuan, China

[3] Center for Psychiatry Research, Zigong Institute of Brain Science, Zigong 643021, Sichuan, China

Corresponding authors: Bo Liu (liubo2511@163.com) and Youguo Tan (13890055464@163.com)

Jianfei Wu, Yu Liu and Yuanyuan Zeng have contributed equally to this work as first authors.

Abstract:

Background The toxic microenvironment after traumatic brain injury (TBI) limits the efficacy of transplanted stem cells. Fisetin, an antioxidant and immunomodulator, holds potential for enhancing cellular stress tolerance. This study aimed to investigate whether preconditioning adipose-derived mesenchymal stem cells (ADSCs) with fisetin could enhance their stress tolerance and promote neural repair in TBI.

Methods *In vitro*, an H_2O_2-induced oxidative stress model was established to evaluate the effects of fisetin on ADSC survival, reactive oxygen species (ROS) production, and the Nrf2/HO-1 pathway. *In vivo*, fisetin-pretreated ADSCs (F-PreSCs) were intranasally transplanted into mice following controlled cortical impact (CCI). The therapeutic effects were assessed by evaluating cortical lesions, neuronal survival, gliosis, macrophage/microglia polarization, and oxidative stress. Behavioral tests, including the modified Neurological Severity Score (mNSS), open field test (OFT), elevated plus maze (EPM), and Morris water maze (MWM), were performed to evaluate sensorimotor and cognitive functions. The biosafety of the treatment was also evaluated.

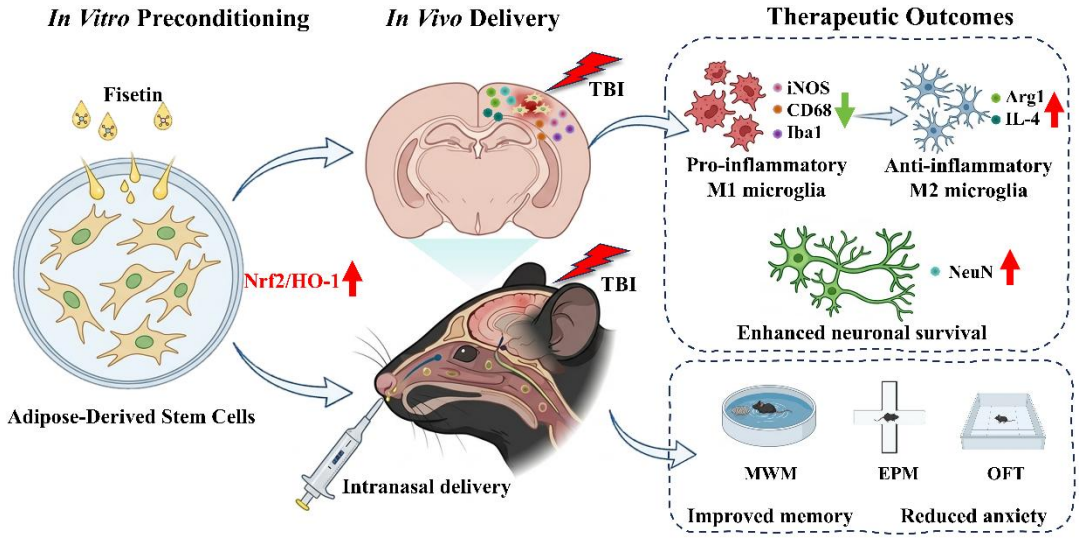
Results *In vitro*, 25 μM fisetin improved ADSC survival, reduced ROS levels, and activated the Nrf2/HO-1 pathway under oxidative stress conditions. *In vivo*, intranasal transplantation of F-PreSCs reduced cortical lesions, rescued NeuN-positive neurons, and attenuated reactive astrogliosis. Furthermore, F-PreSCs promoted the polarization of macrophages/microglia toward the anti-inflammatory M2 phenotype and alleviated oxidative stress in the injured cortex. Behavioral tests demonstrated that F-PreSCs significantly improved sensorimotor and cognitive functions. Notably, no obvious acute toxicity was observed in the treated mice.

Conclusion Fisetin pretreatment enhances ADSC survival under pathological stress, and transplantation of F-PreSCs effectively remodels the post-TBI microenvironment. This "empowered stem cell" strategy offers a safe and promising preconditioning approach for TBI therapy.

Graphical Abstract

Fisetin preconditioning endows adipose-derived mesenchymal stem cells with

Nrf2/HO-1-mediated stress resistance, enabling intranasal F-PreSC transplantation to remodel the post-TBI microenvironment via M2 microglial polarization, neuronal rescue, and improved sensorimotor and cognitive recovery.



Keywords Traumatic brain injury. ADSCs. Fisetin. Microglia. Nrf2/HO-1

Introduction

Traumatic brain injury (TBI) is a complex pathological event induced by external mechanical forces, with global annual cases of nearly 30 million [1, 2]. As the leading cause of death and disability among young adults, TBI not only imposes a substantial socioeconomic burden but also evolves into a chronic health challenge due to its long-term neurological dysfunction [3]. From a pathological perspective, TBI is a cascade process triggered by mechanical insult, characterized by high spatiotemporal heterogeneity [2]. Within hours to days following the initial trauma, the lesion site is immersed in a "toxic microenvironment" characterized by a reactive oxygen species (ROS) burst, excitotoxicity, and immune homeostasis imbalance [4, 5]. This secondary injury amplifies oxidative stress signals, inducing large-scale neuronal apoptosis and diffuse axonal injury, ultimately leading to irreversible cognitive deficits and neurodegenerative pathology [6-8]. The current clinical interventions primarily focus on supportive therapies such as surgical decompression and maintaining vital signs, and are unable to repair damaged neurons or remodel the

neuroinflammatory microenvironment [9, 10]. Therefore, it is urgent to develop strategies that facilitate neural regeneration and microenvironment remodeling.

Regenerative medicine strategies centered on mesenchymal stem cells (MSCs) have provided new therapeutic approaches for central nervous system disorders [11, 12]. In neurodegenerative diseases such as Alzheimer's disease (AD), Parkinson's disease (PD), and amyotrophic lateral sclerosis (ALS) [13, 14], as well as in acute central nervous system injury models such as stroke and spinal cord injury [15, 16], ADSCs have shown remarkable potential in alleviating pathological damage and promoting endogenous repair through their paracrine and immunomodulatory functions. However, the inflammatory and oxidative stress microenvironment at the injury site compromises the survival and functional performance of transplanted stem cells [17, 18]. High concentrations of pro-inflammatory cytokines and oxidative stress often induce premature senescence or programmed death of the transplanted stem cells, leading to a significant reduction of their biological efficacy [17, 19]. Therefore, "preconditioning" stem cells to enhance their ability to resist pathological stress and remodel the microenvironment has become a research hotspot in neural regeneration.

Fisetin, a pleiotropic flavonoid compound, exhibits neuroprotective effects [20, 21]. Fisetin's uniqueness lies in its dual regulatory role: it acts as both an efficient ROS scavenger and a potential senolytic agent [22, 23]. Fisetin not only crosses the blood-brain barrier (BBB) to exert direct effects, but it also enhances cellular antioxidant stress capacity by activating Nrf2 and its downstream antioxidant defense hub, heme oxygenase-1 (HO-1) [23-25]. Furthermore, fisetin promotes the expression of anti-inflammatory factors and enhances the immunomodulatory capacity [26, 27].

Given the outstanding performance of fisetin in enhancing the endogenous defense capacity of cells, this study proposes a "defensive empowerment" strategy: pretreating ADSCs with fisetin *in vitro*. We aim to investigate whether fisetin-pretreated ADSCs (F-PreSCs) can acquire stress resistance, thereby maintaining higher metabolic activity and paracrine efficacy in the extreme TBI microenvironment, ultimately achieving profound repair of neurological deficits and significant improvement of behavioral phenotypes. This approach of empowering

ADSCs through preconditioning offers a new strategy for the treatment of TBI.

Materials and Methods

Experimental Animals

Specific pathogen-free (SPF) male C57BL/6J mice (8–10 weeks old, body weight 20–24 g) were used in this study and purchased from Jicui Yaokang Biotechnology Co., Ltd. (Chengdu, China). The animals were housed in a standard SPF facility under controlled environmental conditions: temperature 22–25 °C, relative humidity 50–60%, light intensity 15–20 lx, and a 12-h light/12-h dark cycle. All mice had free access to food and water. Before the start of experiments, all animals were allowed to acclimate to the housing conditions for at least 7 days.

Mice were euthanized by an intraperitoneal overdose of urethane (1.5 g/kg). Deep anesthesia was confirmed by the loss of corneal and pedal withdrawal reflexes. Under deep anesthesia, mice were transcardially perfused with ice-cold PBS followed by ice-cold 4% paraformaldehyde (PFA) using a standard transcardial perfusion system. For Western blotting, mice were perfused with ice-cold PBS alone. Death was confirmed by the cessation of heartbeat and respiration. At the time of sacrifice after behavioral testing, mice were 10–12 weeks old and weighed 22–28 g. All experimental procedures were approved by the Ethics Committee of Zigong Mental Health Center (Approval No. ZPRC-20250326). All animal experimental procedures followed the "Guide for the Care and Use of Laboratory Animals" published by the National Institutes of Health (NIH). This study strictly adhered to animal welfare and ethical principles.

Isolation and Culture of Mouse ADSCs

Under sterile conditions, inguinal and epididymal adipose tissues were collected from 8-10-week-old mice. After washing with PBS, the tissues were minced into approximately 1 mm^3 pieces and digested with an equal volume of 0.1% collagenase type I in a shaking incubator at 37 °C (120 r/min) for 60 min. Digestion was terminated by adding culture medium containing 10% fetal bovine serum (FBS). The mixture was centrifuged at 1200 r/min for 5 min, the upper layer of floating fat was

removed, and the cell pellet was collected. After resuspension, the cells were filtered through a 70 μm cell strainer. Following centrifugation at 800 r/min for 5 min, the cells were resuspended in DMEM/F12 complete medium containing 10% FBS and 1% penicillin-streptomycin, seeded at a density of 1×10^5 cells/cm^2 in culture flasks, and cultured in a 37 °C incubator with 5% CO_2. After 48 h, the medium was replaced to remove non-adherent cells, and thereafter the medium was changed every 2 days. When the cells reached 80-90% confluence, they were digested using 0.25% trypsin and passaged at a ratio of 1:3. All subsequent experiments were performed using cells at passages 3-5 (P3-P5).

Adipogenic and Osteogenic Differentiation of ADSCs

When P3 cells reached 80-90% confluence (for adipogenic differentiation) or 60-70% confluence (for osteogenic differentiation), the culture medium was replaced with adipogenic induction medium (containing dexamethasone, IBMX, insulin, and FBS) or osteogenic induction medium (containing dexamethasone, β-glycerophosphate, ascorbic acid, and FBS), respectively. During the induction period, the medium was refreshed every 3 days. After 14-21 days of continuous induction, cells were fixed with 4% paraformaldehyde (PFA), and differentiation was assessed by Oil Red O staining (C0158M, Beyotime Biotechnology, China) or Alizarin Red S staining (S5974, Selleck, USA), thereby confirming the multipotent differentiation potential of the ADSCs.

Cytoskeleton Staining of ADSCs

To visualize the cytoskeletal morphology, the ADSCs in the confocal culture dishes were washed twice with PBS and then fixed with 4% PFA solution at room temperature for 15 min. After three washes, the cells were permeabilized with PBS containing 0.1% Triton X-100 for 15 min. Subsequently, the cells were incubated with Actin-Tracker Green (C2201S, Beyotime Biotechnology, China) staining working solution (diluted 1:100) for 45 min at room temperature in the dark, followed by three washes with PBS. After DAPI staining for 15 min, the cells were washed three times with PBS. Cell distribution and morphology were observed under a fluorescence microscope.

Flow Cytometry

The surface markers of P3 ADSCs were characterized by flow cytometry. Cells were digested and resuspended to prepare a single-cell suspension (density approximately 1 × 10^6 cells/mL). Fluorescently labeled monoclonal antibodies against CD34 (FITC), CD73 (PE), CD90 (FITC), and CD105 (PE) were added, and the cells were incubated at 4 °C in the dark for 30 min. After three washes with PBS, data were acquired on a flow cytometer and analyzed using FlowJo software.

CCK-8 Assay

P3 ADSCs were digested, resuspended, and seeded into 96-well plates at a density of 5 × 10^3 cells per well. After culture at 37 °C in a 5% CO_2 incubator for 24 h, subsequent drug treatments were performed. To establish an oxidative stress model, cells were exposed to complete medium containing different concentrations (0, 12.5, 25, 50, 100, 200 μM) of H_2O_2 for 12 h. The concentration that reduced cell viability to approximately 50-60% was selected as the modeling concentration for subsequent experiments. To evaluate the cytotoxicity of fisetin (S2298, Selleck, USA) and identify the optimal concentration with no significant inhibitory effect on cell growth, cells were exposed to medium containing different concentrations (5, 10, 25, 50, 100 μM) of fisetin for 12 h.

Three experimental groups were included: control group (CON), H_2O_2 group (H_2O_2), and H_2O_2 + fisetin group (H_2O_2 + F-Pre). In the H_2O_2 + F-Pre group, cells were pre-incubated with the selected optimal concentration of fisetin for 12 h, followed by stimulation with the 100 μM H_2O_2 for an additional 12 h. After treatment, 10 μL of CCK-8 solution was added to each well, and the plates were incubated in the dark at 37 °C for 2 h. The absorbance (OD value) of each well was measured at 450 nm using a microplate reader, and the cell viability was calculated.

ROS Detection

ADSCs were seeded into confocal culture dishes at a density of 5 × 10^4 cells per well and cultured for 24 h. In the H_2O_2 + F-Pre group, cells were pretreated with 25 μM fisetin for 12 h. Subsequently, except for the control group, all other groups were exposed to 100 μM H_2O_2 for an additional 12 h to induce oxidative stress. After

treatment, cells in each group were incubated with 10 μM DCFH-DA fluorescent probe (S0033S, Beyotime Biotechnology, China) at 37 °C in the dark for 30 min. Following incubation, cells were washed three times with PBS to remove unbound probe. Fluorescence images of each group were immediately captured using a confocal microscope. The mean fluorescence intensity was quantified using ImageJ software to assess the ROS levels.

JC-1 staining

ADSCs were seeded in confocal dishes. After washing with PBS, cells were incubated with JC-1 working solution (1:200) at 37°C for 20 min in the dark, washed twice with staining buffer, and immediately imaged under a confocal microscope. The red/green fluorescence ratio was quantified using ImageJ.

TBI Model and Treatment

A total of 48 male C57BL/6 mice were randomly assigned to 4 groups (CON, TBI, TBI+SCs, TBI+F-PreSCs), with 12 mice per group. All 12 mice per group underwent behavioral testing (n = 12 per group). Following behavioral tests, the 12 mice per group were allocated for tissue analyses as follows: 4 mice were transcardially perfused with 4% paraformaldehyde for H&E and Nissl staining (n = 4 per group); another 4 mice were perfused with 4% paraformaldehyde for immunofluorescence staining (n = 4 per group); and the remaining 4 mice were perfused with PBS for Western blot analysis (n = 4 per group).

The TBI model was established following our laboratory's established protocols [8, 28]. Briefly, mice were anesthetized and fixed in a stereotaxic frame. After routine disinfection, the skin was incised. A 2 mm craniotomy was performed 2 mm posterior to the bregma and 1.5 mm lateral to the midline, preserving meningeal integrity. Subsequently, TBI was induced using a controlled cortical impact (CCI) device. The core impact parameters were set as follows: impact velocity 3.9 m/s, impact depth 1.2 mm, and dwell time 500 ms. Mice in the CON group underwent the same craniotomy and wound closure procedures without any cortical impact. After surgery, all mice were placed on a heating pad until recovery. At 1 hour post-CCI, ADSCs were administered intranasally. Following TBI surgery, mice in the TBI + SCs and

TBI + F-PreSCs groups were treated with untreated ADSCs and F-PreSCs, respectively, at a dose of 1×10^6 cells in 10 μL PBS per mouse, delivered as 5 μL per nostril alternately, with the mouse kept supine for 2 minutes after administration. The treatment was given twice at a 7-day interval. Mice in the con and TBI groups received an equal volume of sterile saline intranasally.

Animal Behavioral Tests

The animal behavioral test protocols were based on previous studies [28-30]. To ensure accuracy, all tests were conducted in a quiet environment. Mice were transferred to the behavioral laboratory 1 h before the test to minimize transport stress. After each mouse was tested, the apparatus was cleaned with 75% ethanol to eliminate residual odors, and the next mouse was tested after the ethanol had evaporated.

The Modified Neurological Severity Score (mNSS) was used to evaluate neurological recovery in TBI mice. Assessments were performed under double-blind conditions by trained experimenters. The test comprehensively included four domains: motor function, sensory response, balance ability, and abnormal reflexes. The total score ranged from 0 to 18. The higher score indicated a more severe neurological impairment.

The Open Field Test (OFT) was used to assess spontaneous locomotor activity and anxiety-like behavior. The apparatus was an open-top square box ($40 \times 40 \times 40$ cm^3). The bottom area was divided into a central zone and a peripheral zone. During testing, each mouse was gently placed in the center of the area and allowed to explore freely for 10 min. A video tracking system recorded the number of entries into the central zone and the residence time in the central zone.

The Elevated Plus Maze (EPM) was used to further evaluate anxiety-like behavior. The maze consisted of two open arms, two closed arms, and a central connecting platform. At the start of the test, the mouse was placed on the central platform facing an open arm. The frequency of entries into the open arms and the total time in the open arms were recorded over a 5-min period using a video tracking system.

The Morris Water Maze (MWM) was used to assess spatial learning and memory abilities. The apparatus was a circular pool (diameter 150 cm, height 60 cm). The water was made opaque by the addition of titanium dioxide to enable tracking of the movement trajectory. The pool was divided into four equal quadrants, with a hidden platform (diameter 15 cm) fixed in quadrant I and submerged 2 cm below the water surface. The test was conducted for 5 days, with each mouse receiving three trials per day from random starting points. The escape latency was recorded, with a maximum trial duration of 90 s. If a mouse failed to find the platform within 90 s, it was gently guided to the platform by the experimenter and allowed to remain there for 15 s to reinforce spatial memory. On day 6, the test was performed with the platform removed. The time spent in the target quadrant (the original platform quadrant) and the number of crossings over the former platform location were analyzed using a video tracking system as core measures of spatial memory performance.

H&E Staining

After the behavioral experiments were completed, mice were intraperitoneally injected with urethane (1.5 g/kg, i.p.). Once deep anesthesia was confirmed, the brain, heart, liver, spleen, lung, kidney, and other tissues were immediately collected for subsequent histopathological and molecular biological analyses. The fixed tissues (heart, liver, spleen, lung, and kidney) were embedded in paraffin and serially sectioned at a thickness of 5 μm. The sections were baked at 60 °C, then deparaffinized in xylene and rehydrated through a graded ethanol series. Subsequently, the sections were stained with hematoxylin solution for 5 min, rinsed in water, differentiated in acid-ethanol, and blued in ammonia water. The sections were then dehydrated in 85% and 95% ethanol, counterstained with eosin solution for 5 min. The sections were completely dehydrated in absolute ethanol, cleared in xylene, and mounted with neutral balsam. All sections were observed under an inverted microscope, and images were captured for histopathological evaluation.

Nissl Staining

After behavioral tests, mice were transcardially perfused with PBS and 4% PFA. The brains were collected, fixed in 4% PFA, and then sequentially dehydrated in 10%,

20%, and 30% sucrose solutions (24 h each). The tissues were embedded in OCT for frozen sectioning. Sections from the injury core region were selected and stained using a Nissl staining kit (G1434, Solarbio, China) according to the manufacturer's instructions. After dehydration and clearing, the sections were mounted with neutral resin. Images were acquired using a Nikon Ti2-u microscope, and Nissl-positive neurons were quantitatively counted using ImageJ software to assess the integrity of neuronal structures.

Immunofluorescence Staining

Brain tissues were fixed in 4% PFA for 48 h and then sequentially dehydrated in 10%, 20%, and 30% sucrose solutions (24 h each). Frozen sections (20 μm thick) were prepared from the region with the most severe injury. Cultured ADSCs were washed with PBS and fixed with 4% PFA for 30 min at room temperature. Samples (tissue sections or cells) were permeabilized with 0.5% Triton X-100 for 20 min and then blocked with 5% BSA (SW3015, Solarbio, China) for 40 min at room temperature. Subsequently, the samples were incubated with specific primary antibodies (see Table 1) overnight at 4 °C. The next day, the species-specific fluorescent secondary antibodies were added and incubated for 2 h at room temperature. Nuclei were counterstained with DAPI for 15 min. After staining, the samples were thoroughly washed with PBS and mounted with an anti-fade mounting medium. Fluorescence images were acquired using a Nikon C2 laser confocal microscope, and fluorescence intensities were quantitatively analyzed using ImageJ software.

Western Blotting

All samples were thoroughly homogenized in RIPA lysis buffer containing protease and phosphatase inhibitors. After centrifugation at 12,000 rpm for 15 min at 4 °C, the supernatants were collected. Protein concentrations were precisely quantified using a BCA assay kit. Equal amounts of protein (15 μg per lane) were mixed with loading buffer. The proteins were separated by SDS-PAGE and then transferred onto PVDF membranes (IPVH00010, Merck Millipore). The membranes were blocked with 5% BSA/TBST buffer for 1 h at room temperature, followed by incubation with specific primary antibodies (see Table 1) overnight at 4 °C. The next day, after thorough

washing with TBST, the membranes were incubated with the corresponding secondary antibodies (diluted 1:5000) for 2 h at room temperature. Signals were developed using West Pico ECL chemiluminescent substrate and imaged with a Vilber FUSION Fx6 imaging system. Band intensities were quantified using ImageJ software. Target protein expression levels were normalized to GAPDH to calculate the relative expression of each protein.

Statistical Analysis

Data were analyzed using SPSS 20.0 and plotted with GraphPad Prism 8.02. Results are presented as mean ± SEM. Comparisons among multiple groups were performed using one-way analysis of variance (ANOVA) and Tukey's post hoc test. Statistical significance was defined as $*p < 0.05$, $**p < 0.01$, $***p < 0.001$.

Results

Isolation, Culture, and Surface Marker Characterization of ADSCs

To validate the multipotency and purity of ADSCs, we systematically assessed their morphological features and phenotypes. As shown in the bright-field images in Fig. 1A, ADSCs at P3 exhibited a typical fibroblast-like or spindle-shaped morphology. Multilineage differentiation assays demonstrated that these cells successfully differentiated into osteoblasts and adipocytes: Alizarin Red S staining revealed abundant red calcified nodules (Fig. 1B), while Oil Red O staining clearly showed intracellular accumulation of red lipid droplets (Fig. 1C). Furthermore, Actin/DAPI double staining (Fig. 1D) revealed a well-spread and regularly arranged microfilament cytoskeletal network. Flow cytometry analysis (Fig. 1E) showed that the isolated cells highly expressed the classical mesenchymal stem cell surface markers CD73 (98.4%), CD90 (98.5%), and CD105 (99.3%), while minimally expressing the hematopoietic stem cell marker CD34 (3.78%). These results confirm that we successfully obtained ADSCs with high purity and multipotency.

Fisetin Pretreatment Significantly Attenuated H_2O_2-induced Oxidative Stress Injury in ADSCs

To establish an oxidative stress model of ADSCs and determine the optimal

intervention concentration of fisetin, we first evaluated the effects of different drug concentrations on cell viability using the CCK-8 assay. As shown in Fig. 2A, H_2O_2 exerted a significant dose-dependent toxicity on ADSCs, with cell viability decreasing markedly at concentrations of 100 and 200 μM. Notably, 100 μM H_2O_2 reduced cell survival to approximately 50% and was therefore selected as the concentration for establishing the oxidative stress model in subsequent experiments. On the other hand, fisetin at concentrations ranging from 5-50 μM exhibited no obvious cytotoxicity to ADSCs; however, cell viability decreased significantly at 100 μM. Although 25 μM fisetin did not significantly promote ADSC proliferation compared to the control group, it was the highest concentration that did not exhibit any inhibitory effect on cell viability. Given that concentrations ≥50 μM showed a declining trend, 25 μM was selected as the optimal concentration for subsequent preconditioning experiments (Fig. 2B). We found that pretreatment with 25 μM fisetin (F-Pre) significantly inhibited H_2O_2-induced cell death (Fig. 2C). The ROS fluorescent probe staining (Fig. 2D) and corresponding quantitative analysis (Fig. 2F) showed that the control (CON) group exhibited low intracellular ROS levels, whereas H_2O_2 exposure led to ROS accumulation. Importantly, fisetin pretreatment significantly reduced the excessive intracellular ROS, resulting in a marked decrease in fluorescence intensity. Furthermore, JC-1 staining (Fig. 2E) revealed that H_2O_2 induced mitochondrial membrane potential collapse, as evidenced by increased green fluorescence (monomers) and decreased red fluorescence (aggregates), while fisetin pretreatment largely preserved mitochondrial membrane potential. Quantitative results of the JC-1 red/green ratio (Fig. 2G) showed that fisetin pretreatment significantly attenuated H_2O_2-induced mitochondrial depolarization.

Fisetin Pretreatment Enhanced Antioxidant Capacity via the Nrf2/HO-1 Pathway in ADSCs

To elucidate the molecular mechanism by which fisetin enhances the stress tolerance of ADSCs, we evaluated the expression levels of the antioxidant enzyme HO-1 and the transcription factor Nrf2 by immunofluorescence (Fig. 3). As shown in Fig. 3A and 3B, the HO-1 fluorescence intensity in the H_2O_2 + F-Pre group was significantly

higher than that in the H_2O_2 group. Similarly, the expression of Nrf2 was also markedly upregulated following fisetin pretreatment (Fig. 3C-D). These results demonstrate that fisetin pretreatment comprehensively enhances the survival capacity of ADSCs in an oxidative stress environment by activating the Nrf2/HO-1 signaling pathway.

Transplantation of F-PreSCs Significantly Reduced Brain Lesions and Rescued Neurons in TBI Mice

We transplanted F-PreSCs into TBI mice to evaluate their neuroprotective effect. H&E staining (Fig. 4A) showed that the TBI group exhibited extensive tissue loss and cell necrosis in the injured cerebral cortex. Following ADSC transplantation, the cortical lesion volume was reduced to varying degrees, with the most pronounced restoration of tissue integrity observed in the TBI + F-PreSCs group. Nissl staining (Fig. 4B) and quantification of Nissl-positive cells (Fig. 4C) further confirmed that TBI caused severe loss of Nissl bodies in the peri-lesion area; F-PreSCs effectively rescued this degenerative change, and their reparative effect was significantly superior to that of untreated ADSCs. Moreover, immunofluorescence staining for the specific mature neuronal marker NeuN (Fig. 4D) and quantitative analysis of fluorescence intensity (Fig. 4E) consistently demonstrated that F-PreSCs transplantation more effectively inhibited trauma-induced apoptosis of NeuN-positive neurons.

F-PreSCs Effectively Inhibited Glial Overactivation and Neuroinflammation Following TBI

Neuroinflammation and reactive gliosis are key pathological factors that exacerbate secondary injury. Immunofluorescence staining for the microglia/macrophage markers Iba1 (Fig. 5A) and CD68 (Fig. 5C) revealed that TBI triggered a robust inflammatory response. Quantitative results showed that the fluorescence intensities of Iba1 (Fig. 5B) and CD68 (Fig. 5D) in the TBI group were significantly increased compared with the control group. ADSC treatment partially alleviated the inflammation, whereas F-PreSCs exhibited superior anti-inflammatory capacity, further significantly downregulating the expression levels of Iba1 and CD68. Meanwhile, GFAP staining for astrocytes (Fig. 6A) and its quantification (Fig. 6B) revealed that TBI caused a

marked increase in GFAP expression in the lesion area. The F-PreSCs group suppressed this increase more effectively than the SCs group, indicating that F-PreSCs more potently attenuated reactive astrogliosis.

F-PreSCs Effectively Improved the Neural Microenvironment in TBI Mice

To further investigate the molecular mechanisms by which F-PreSCs improve the microenvironment, we extracted proteins from the ipsilateral brain tissue and conducted comprehensive Western blot analysis (Fig. 6C). Relative quantification results (Fig. 6D-I) showed that TBI markedly increased the expression of the pro-inflammatory/M1-type marker iNOS (Fig. 6D) and IL-6 (Fig. 6H), while F-PreSCs suppressed these increases more effectively than SCs. The anti-inflammatory/M2-type macrophage marker Arg1 (Fig. 6E) and the key anti-inflammatory cytokine IL-4 (Fig. 6I) were downregulated in the TBI group. However, the expression levels of Arg1 and IL-4 were significantly upregulated in the F-PreSCs group, and the extent of upregulation was markedly greater than that in the SCs group. Notably, TBI reduced the expression levels of HO-1 (Fig. 6G); however, the expression levels of HO-1 were markedly upregulated after F-PreSCs treatment, suggesting that the oxidative stress microenvironment at the lesion area was substantially attenuated. Moreover, the NeuN protein level detected by Western blot (Fig. 6F) further corroborated the immunofluorescence results, confirming the robust neuronal rescue capacity of F-PreSCs.

F-PreSCs Comprehensively Improved TBI-induced Sensorimotor Deficits and Cognitive Impairments, with Favorable Biosafety

In the OFT, which assesses anxiety-like behavior and exploratory activity, TBI mice exhibited avoidant behavior. In contrast, the F-PreSCs group showed significantly increased numbers of entries into the central zone (Fig. 7A) and longer residence time in the central zone (Fig. 7B). In the EPM test, F-PreSCs significantly increased the frequency of entries into the open arms (Fig. 7C) and prolonged the time in the open arms (Fig. 7D), strongly demonstrating their anti-anxiety effect. Spatial learning and memory were evaluated using the MWM. Across training days, the F-PreSCs group exhibited significantly shortened escape latencies (Fig. 7E) compared with the TBI

group. In the probe trial after platform removal, the F-PreSCs group showed a marked recovery in the number of platform crossings (Fig. 7F) and the percentage of time in the target quadrant (Fig. 7G). Furthermore, the results of mNSS (Fig. 7H) indicated that F-PreSCs significantly improved sensorimotor function in TBI mice.

Finally, we systematically examined major organs (heart, liver, spleen, lung, and kidney) by H&E histopathological analysis (Fig. 8) and observed no inflammatory infiltration or histomorphological abnormalities, indicating a favorable preliminary safety profile of F-PreSCs therapy under the current experimental conditions.

Discussion

TBI is not only a primary mechanical insult but also a long-term process driven by oxidative stress, neuroinflammation, and metabolic dysregulation [2, 28]. Our results demonstrate that fisetin pretreatment significantly enhances the anti-apoptotic and antioxidant capacities of ADSCs under oxidative stress *in vitro*. More importantly, F-PreSCs were associated with remodeling of the pathological microenvironment at the lesion site in TBI mice, as evidenced by attenuated reactive astrogliosis, promotion of microglial/macrophage polarization toward the M2 anti-inflammatory phenotype, and rescue of dying neurons. These findings provide novel molecular insights into the therapeutic potential of stem cell preconditioning strategies and establish a theoretical foundation for clinical translation in TBI. The "microenvironment" formed at the injury site after TBI, characterized by excessive ROS and pro-inflammatory cytokines, is the primary cause of early death of transplanted stem cells [16, 31].

In this study, we observed that treatment with 100 μM H_2O_2 reduced ADSC viability to approximately 50%, successfully simulating this pathological stress. Under these conditions, fisetin pretreatment exhibited remarkable cytoprotective effects. Notably, the protective effect of fisetin is not solely derived from its free radical scavenging activity. Further mechanistic analysis revealed that fisetin pretreatment significantly upregulated the expression of Nrf2 and HO-1 in ADSCs. Nrf2 is a transcription factor that regulates the activation of numerous cytoprotective

genes, including HO-1. HO-1 is a key antioxidant enzyme that maintains cellular redox homeostasis. [32, 33]. Therefore, we propose that fisetin exerts a protective effect on ADSCs by activating the Nrf2/HO-1 pathway.

Neuroinflammation is a central driver of secondary injury after TBI [28]. In this study, TBI model mice exhibited extensive infiltration of $Iba1^{+}/CD68^{+}$ microglia/macrophages in the injured cortex, accompanied by a significant increase in $GFAP^{+}$ astrocytes, indicating uncontrolled inflammation and reactive astrogliosis. However, F-PreSCs transplantation not only significantly suppressed the expression of these inflammatory markers but also induced a profound immunological phenotype switch. Western blot results showed that in the F-PreSCs group, the M1-type marker iNOS was potently inhibited, whereas the expression of the M2-type marker Arg1 and the anti-inflammatory cytokine IL-4 was substantially upregulated. This “M1-to-M2 switch” has important pathological implications: M2 macrophages secrete cytokines such as IL-10 and TGF-β, which promote tissue repair while inhibiting the formation of dense glial scars [34, 35]. Notably, although the untreated SCs group also exhibited a certain anti-inflammatory effect, its efficacy was far lower than that of the F-PreSCs group. This suggests that fisetin pretreatment, possibly through epigenetic reprogramming (e.g., histone acetylation or DNA methylation modifications), enables ADSCs to exert immunomodulatory effects persistently and efficiently, thereby achieving “precise regulation” of the immune microenvironment [36, 37].

As a core antioxidant enzyme, HO-1 generates metabolites with anti-inflammatory and anti-apoptotic effects by degrading heme, and also plays a key role in maintaining cellular redox homeostasis [5, 32]. In this study, we found that fisetin pretreatment directly upregulated HO-1 protein expression in ADSCs, and after intranasal transplantation of F-PreSCs, the downregulated HO-1 expression in the injured brain tissue of TBI mice was also significantly elevated. This reveals the neuroprotective mechanism of F-PreSCs: on one hand, fisetin activates the Nrf2/HO-1 pathway in ADSCs, endowing them with the inherent advantage of high HO-1 expression before entering the lesion site, thereby resisting early death induced by oxidative stress [38, 39]; on the other hand, transplantation of ADSCs promoted

microglial polarization toward the M2 phenotype, which may be primarily attributable to paracrine effects of the transplanted ADSCs (including anti-inflammatory factors and exosomes)[40, 41]. Moreover, fisetin pretreatment enhanced the resistance of ADSCs to oxidative stress, thereby reducing apoptosis and ultimately promoting the secretion of more anti-inflammatory factors and exosomes. This M2 polarization was associated with elevated HO-1 expression, establishing an anti-inflammatory and antioxidant positive feedback loop that ultimately restores redox homeostasis within the microenvironment [42-44]. Collectively, these findings suggest that F-PreSCs may exert neuroprotective effects through a synergistic mechanism involving self-protection and microenvironment remodeling. The upregulation of Nrf2/HO-1 expression and its associated antioxidant response represent key determinants of its therapeutic efficacy. However, we acknowledge that definitive causal attribution to the Nrf2/HO-1 pathway requires further loss-of-function studies.

The ultimate goal of neural repair is functional recovery. In this study, we employed a multidimensional behavioral assessment framework covering emotional state (OFT, EPM), sensorimotor function (mNSS), and higher-order cognition (MWM). The results showed that the F-PreSCs group exhibited significant improvements in residence time in the central area of the OFT, the frequency of entries into the open arms in the EPM, and the number of platform crossings in the MWM. Notably, the therapeutic efficacy of F-PreSCs was superior not only to the TBI group but also to the SCs group [28]. This suggests that stem cells with a “stress-resistant empowered” phenotype can survive and exert sufficient neuroremodeling effects within the complex post-TBI pathological environment, thereby improving spatial memory and anxiety-like behaviors [45, 46].

Furthermore, this study employed intranasal delivery for stem cell transplantation. Compared with stereotactic injection or intravenous infusion, intranasal administration offers significant advantages, including non-invasiveness, repeatability, BBB bypass, and brain-targeted delivery [47, 48]. Our pathological results confirmed that neither untreated nor pretreated ADSCs caused any structural abnormalities or inflammatory infiltration in major organs, including the heart, liver,

spleen, lung, and kidney, demonstrating the high *in vivo* biosafety of this therapeutic approach. This is particularly critical for advancing clinical translation.

Several limitations of this study should be acknowledged. First, the proposed role of the Nrf2/HO-1 pathway in F-PreSC-mediated neuroprotection is primarily supported by correlative evidence; we did not perform pharmacological inhibition or genetic knockdown experiments to establish definitive causality. Second, our assessment of reactive gliosis was based on GFAP expression, which reflects astrocytic activation but does not fully capture the complexity of glial scar formation involving extracellular matrix components such as chondroitin sulfate proteoglycans. Third, the biosafety evaluation was limited to histopathological examination of major organs, without long-term tumorigenicity or immunogenicity assessment. In future studies, it is necessary to employ loss-of-function approaches, glial scar formation assays, and long-term safety evaluations.

Conclusions

In summary, fisetin pretreatment enhances the antioxidant and paracrine efficacy of ADSCs, thereby effectively attenuating the “inflammatory-oxidative” cascade after TBI. This "empowered stem cell" strategy not only enhances the stress tolerance and survival of transplanted cells within harsh microenvironments but also offers a novel therapy for central nervous system injuries. Nevertheless, future studies should further employ single-cell sequencing or spatial transcriptomics to deeply dissect the complex molecular networks between F-PreSCs and endogenous brain cells.

Author contributions

J.W., Y.L. and Y.Z.: Conceptualization, Data curation, Formal analysis, Methodology, Project administration, Visualization and Writing - original & draft. Y.T. and B.L.: Project administration, Validation, Writing - review & editing, Funding acquisition and Resources. All authors read and approved the final study manuscript. All authors reviewed the manuscript.

Funding

This work was supported by grants from the the Health Commission of Sichuan Province Medical

Science and Technology Program (26WSQNMP027); Zigong Key Science and Technology Plan Project (2026YLWS25); Zigong Key Science and Technology Plan (Collaborative Innovation Project of Zigong Institute of Brain Sciences) (2023-NKY-01-02, 2025NKY0104 and 2025NKY0201); Zigong Municipal Natural Science Research Project (2026Y02); Collaborative Innovation Project of Zigong Integrated Traditional Chinese and Western Medicine Research Institute (2025ZXY0206); Collaborative Innovation Project of Zigong Medical Big Data and Artificial Intelligence Research Institute (2024-YGY-02-04 and 2026YGY0204) and Scientific Research Project of Zigong Health Commission (22yb001, 24zd008 and 24yb067).

Declarations

Conflict of interest

The authors have no financial conflicts of interest.

Data availability

The data that support the findings of this study are available on request from the corresponding author.

Ethical Approval

All experimental procedures were approved by the Ethics Committee of Zigong Mental Health Center (Approval No. ZPRC-20250326). All animal experimental procedures followed the "Guide for the Care and Use of Laboratory Animals" published by the National Institutes of Health (NIH). This study strictly adhered to animal welfare and ethical principles.

References

1. Guan B, Anderson DB, Chen L, et al. (2023) Global, regional and national burden of traumatic brain injury and spinal cord injury, 1990-2019: a systematic analysis for the Global Burden of Disease Study 2019. BMJ open 13:e075049. doi:10.1136/bmjopen-2023-075049
2. Li N, Lu W, Tang L, et al. (2025) Microglia in Post-Traumatic Brain Injury (TBI) Cognitive Impairment: From Pathological Changes to Therapeutic Approaches. CNS neuroscience & therapeutics 31:e70568. doi:10.1111/cns.70568
3. Allen BC, Cummer E, Sarma AK (2023) Traumatic Brain Injury in Select Low- and Middle-Income Countries: A Narrative Review of the Literature. Journal of neurotrauma 40:602-619. doi:10.1089/neu.2022.0068
4. Thapa K, Khan H, Singh TG, et al. (2021) Traumatic Brain Injury: Mechanistic Insight on Pathophysiology and Potential Therapeutic Targets. Journal of molecular neuroscience : MN 71:1725-1742. doi:10.1007/s12031-021-01841-7
5. Zhao P, Wei Y, Sun G, et al. (2022) Fetuin-A alleviates neuroinflammation against traumatic brain injury-induced microglial necroptosis by regulating Nrf-2/HO-1 pathway. Journal of

neuroinflammation 19:269. doi:10.1186/s12974-022-02633-5

6. Weng W, He Z, Ma Z, et al. (2025) Tufm lactylation regulates neuronal apoptosis by modulating mitophagy in traumatic brain injury. Cell death and differentiation 32:530-545. doi:10.1038/s41418-024-01408-0
7. Sharma B, Monteiro L, Changoor A, et al. (2025) The Scale of Neurodegeneration in Moderate-to-Severe Traumatic Brain Injury: A Systematic Review of Longitudinal Studies. Annals of neurology 98:668-681. doi:10.1002/ana.27279
8. Wu J, Wang B, Tan Y, et al. (2025) Ligustilide Ameliorates Traumatic Brain Injury in Aged Mice by Attenuating Microglia-Mediated Neuroinflammation. Neurochemical research 50:309. doi:10.1007/s11064-025-04560-2
9. Mohammed FS, Omay SB, Sheth KN, et al. (2023) Nanoparticle-based drug delivery for the treatment of traumatic brain injury. Expert opinion on drug delivery 20:55-73. doi:10.1080/17425247.2023.2152001
10. He X, Lei M, Chen X, et al. (2025) Dynamic Hydrogel-Based Strategy for Traumatic Brain Injury Modeling and Therapy. CNS neuroscience & therapeutics 31:e70148. doi:10.1111/cns.70148
11. Ghasemi M, Roshandel E, Mohammadian M, et al. (2023) Mesenchymal stromal cell-derived secretome-based therapy for neurodegenerative diseases: overview of clinical trials. Stem cell research & therapy 14:122. doi:10.1186/s13287-023-03264-0
12. Shan Y, Zhang M, Tao E, et al. (2024) Pharmacokinetic characteristics of mesenchymal stem cells in translational challenges. Signal transduction and targeted therapy 9:242. doi:10.1038/s41392-024-01936-8
13. Han F, Lu P (2020) Introduction for Stem Cell-Based Therapy for Neurodegenerative Diseases. Advances in experimental medicine and biology 1266:1-8. doi:10.1007/978-981-15-4370-8_1
14. Temple S (2023) Advancing cell therapy for neurodegenerative diseases. Cell stem cell 30:512-529. doi:10.1016/j.stem.2023.03.017
15. Martirosyan NL (2021) Pharmacologic and Cell-Based Therapies for Acute Spinal Cord Injury. Neurosurgery clinics of North America 32:389-395. doi:10.1016/j.nec.2021.03.010
16. Li X, Sundström E (2022) Stem Cell Therapies for Central Nervous System Trauma: The 4 Ws-What, When, Where, and Why. Stem cells translational medicine 11:14-25. doi:10.1093/stcltm/szab006
17. Tang X, Deng P, Li L, et al. (2024) Advances in genetically modified neural stem cell therapy for central nervous system injury and neurological diseases. Stem cell research & therapy 15:482. doi:10.1186/s13287-024-04089-1
18. Jiang EY, Wang K, Zhang QZ, et al. (2025) H_2O_2 preconditioning enhances the transplantation-mediated therapeutic effect of bone marrow-derived mesenchymal stem cells after traumatic brain injury. International immunopharmacology 161:115018. doi:10.1016/j.intimp.2025.115018
19. Wen J, Yi L, Chen L, et al. (2025) Short-Term DMOG treatment rejuvenates senescent mesenchymal stem cells by enhancing mitochondrial function and mitophagy through the HIF-1α/BNIP3 pathway. Stem cell research & therapy 16:274. doi:10.1186/s13287-025-04422-2
20. Imran M, Saeed F, Gilani SA, et al. (2021) Fisetin: An anticancer perspective. Food science & nutrition 9:3-16. doi:10.1002/fsn3.1872

21. Bjørklund G, Oliinyk P, Khavrona O, et al. (2025) The Effects of Fisetin and Curcumin on Oxidative Damage Caused by Transition Metals in Neurodegenerative Diseases. Molecular neurobiology 62:1225-1246. doi:10.1007/s12035-024-04321-2
22. Yousefzadeh MJ, Zhu Y, McGowan SJ, et al. (2018) Fisetin is a senotherapeutic that extends health and lifespan. EBioMedicine 36:18-28. doi:10.1016/j.ebiom.2018.09.015
23. Wei HK, Qi JJ, Wang YQ, et al. (2025) Fisetin alleviates oxidative stress and promotes porcine early embryonic development via activation of the NRF2-ARE signalling pathway. Animal bioscience 38:1160-1174. doi:10.5713/ab.24.0691
24. Rakshit D, Goyal R, Yadav V, et al. (2024) Nanoformulated fisetin ameliorates Alzheimer's disease via reducing proinflammatory cytokines and activating the NRF2/HO-1 pathway. Nanomedicine (London, England) 19:2537-2553. doi:10.1080/17435889.2024.2419814
25. Li C, Zhang Y, Deng Y, et al. (2024) Fisetin suppresses ferroptosis through Nrf2 and attenuates intervertebral disc degeneration in rats. European journal of pharmacology 964:176298. doi:10.1016/j.ejphar.2023.176298
26. Wu SJ, Huang WC, Cheng CY, et al. (2022) Fisetin Suppresses the Inflammatory Response and Oxidative Stress in Bronchial Epithelial Cells. Nutrients 14. doi:10.3390/nu14091841
27. Jiang Y, Guo J, Yang Y, et al. (2025) Fisetin Augments OEC Neuroprotection Through Modulating Neurotrophin/Cytokine Signaling and Activating PI3K/Akt/CREB Pathway in an In Vitro Neurodegenerative Injury. Neuromolecular medicine 27:66. doi:10.1007/s12017-025-08888-4
28. Wu J, Tang Y, Wang Y, et al. (2026) Ganoderic Acid a Promotes Functional Recovery After Traumatic Brain Injury By Protecting Blood-brain Barrier Integrity and Modulating Microglial Polarization. Journal of neuroimmune pharmacology : the official journal of the Society on NeuroImmune Pharmacology 21. doi:10.1007/s11481-026-10289-8
29. Wu J, Liu Y, Wang B, et al. (2025) A potential strategy for improving offspring behavior in maternal immune activation: Amantadine-mediated suppression of neuroinflammation. Animal models and experimental medicine 8:1836-1850. doi:10.1002/ame2.70059
30. Wu J, Zhou Y, Liu Y, et al. (2026) A smart polyhydroxyalkanoate-hyaluronic acid hybrid biphasic delivery platform for enhanced Alzheimer’s symptom management via sustained huperzine A release. 57:102-120. doi:10.22203/eCM.v057a05
31. Huang D, Siaw-Debrah F, Wang H, et al. (2020) Transplanting Rac1-silenced bone marrow mesenchymal stem cells promote neurological function recovery in TBI mice. Aging 13:2822-2850. doi:10.18632/aging.202334
32. Silva R, Vasconcelos LR, Travassos LH (2022) The different facets of heme-oxygenase 1 in innate and adaptive immunity. Cell biochemistry and biophysics 80:609-631. doi:10.1007/s12013-022-01087-z
33. Tonelli C, Chio IIC, Tuveson DAJA, et al. (2018) Transcriptional regulation by Nrf2. 29:1727-1745.
34. Fei M, Wang H, Zhou M, et al. (2020) Podoplanin influences the inflammatory phenotypes and mobility of microglia in traumatic brain injury. Biochemical and biophysical research communications 523:361-367. doi:10.1016/j.bbrc.2019.12.003
35. Lu Y, Yin H, Lou L, et al. (2026) M2 polarization of macrophages: Manipulation of spinal cord injury repair. Neural regeneration research 21:4195-4210. doi:10.4103/nrr.Nrr-d-24-01579

36. Kim HJ, Kim SH, Yun JM (2012) Fisetin inhibits hyperglycemia-induced proinflammatory cytokine production by epigenetic mechanisms. Evidence-based complementary and alternative medicine : eCAM 2012:639469. doi:10.1155/2012/639469
37. Afroze N, Alagal RI, Almousa LA, et al. (2026) Fisetin Suppresses the Proliferative and Migratory Behavior of HeLa Cells by Modulating Aberrant Epigenetic Marks (Writers and Erasers). Epigenomes 10. doi:10.3390/epigenomes10010003
38. Zhang H, Zheng W, Feng X, et al. (2019) Nrf2⁻ARE Signaling Acts as Master Pathway for the Cellular Antioxidant Activity of Fisetin. Molecules (Basel, Switzerland) 24. doi:10.3390/molecules24040708
39. Chen M, Jiang Y, Yu H, et al. (2025) Hydrogen Sulfide-Preconditioned Mesenchymal Stem Cells Attenuate Ferroptosis in Corneal Alkali Burn via the AMPK/Nrf2/HO-1 Pathway in an IL-10-Dependent Manner. Investigative ophthalmology & visual science 66:58. doi:10.1167/iovs.66.12.58
40. Hay AJ, Latham AS, Mumford G, et al. (2023) Intranasally delivered mesenchymal stromal cells decrease glial inflammation early in prion disease. 17:1158408.
41. Teo KYW, Zhang S, Loh JT, et al. (2023) Mesenchymal stromal cell exosomes mediate M2-like macrophage polarization through CD73/ecto-5′-nucleotidase activity. 15:1489.
42. Sierra-Filardi E, Vega MA, Sánchez-Mateos P, et al. (2010) Heme Oxygenase-1 expression in M-CSF-polarized M2 macrophages contributes to LPS-induced IL-10 release. Immunobiology 215:788-795. doi:10.1016/j.imbio.2010.05.020
43. Zhang R, Liu Y, Yan K, et al. (2013) Anti-inflammatory and immunomodulatory mechanisms of mesenchymal stem cell transplantation in experimental traumatic brain injury. Journal of neuroinflammation 10:106. doi:10.1186/1742-2094-10-106
44. Bhowmick S, D'Mello V, Caruso D, et al. (2019) Traumatic brain injury-induced downregulation of Nrf2 activates inflammatory response and apoptotic cell death. Journal of molecular medicine (Berlin, Germany) 97:1627-1641. doi:10.1007/s00109-019-01851-4
45. Tye KM, Prakash R, Kim SY, et al. (2011) Amygdala circuitry mediating reversible and bidirectional control of anxiety. Nature 471:358-362. doi:10.1038/nature09820
46. Spellman T, Rigotti M, Ahmari SE, et al. (2015) Hippocampal-prefrontal input supports spatial encoding in working memory. Nature 522:309-314. doi:10.1038/nature14445
47. Drath I, Richter F, Feja M (2025) Nose-to-brain drug delivery: from bench to bedside. Translational neurodegeneration 14:23. doi:10.1186/s40035-025-00481-w
48. Habiba UE, Sathyanarayanan R, Shamim S, et al. (2026) Intranasal administration of stem cells and their derivatives for neurological and respiratory disorders: a systematic review of human clinical trials. Frontiers in aging neuroscience 18:1834543. doi:10.3389/fnagi.2026.1834543

Table 1 Antibody information

Antibody name	Company	Catalog No.	Source	Dilution
CD34	Invitrogen	11-0341-82	Mouse	Flow:1:100
CD73	Invitrogen	12-0731-82	Rat	Flow:1:150
CD90	Invitrogen	11-0900-81	Mouse	Flow:1:800
CD105	Invitrogen	12-1051-82	Rat	Flow:1:40
HO-1	Proteintech	10701-1-AP	Rabbit	IF:1:300; WB:1:5000
NeuN	Cell Signaling Technology	#24307	Mouse	IF:1:500; WB:1:1000
Nrf2	Cell Signaling Technology	# 12721	Rabbit	IF:1:400
Iba1	Cell Signaling Technology	#17198	Rabbit	IF:1:200
CD68	Cell Signaling Technology	#97778	Rabbit	IF:1:800
GFAP	Cell Signaling Technology	#80788	Rabbit	IF:1:200
IL-4	Proteintech	66142-1-Ig	Mouse	WB:1:1000
iNOS	Cell Signaling Technology	#13120	Rabbit	WB:1:1000
Arg1	Cell Signaling Technology	#93668	Rabbit	WB:1:1000
IL-6	Proteintech	21865-1-AP	Rabbit	WB:1:1000
GAPDH	Bioss	bsm-52262R	Rabbit	WB:1:20000

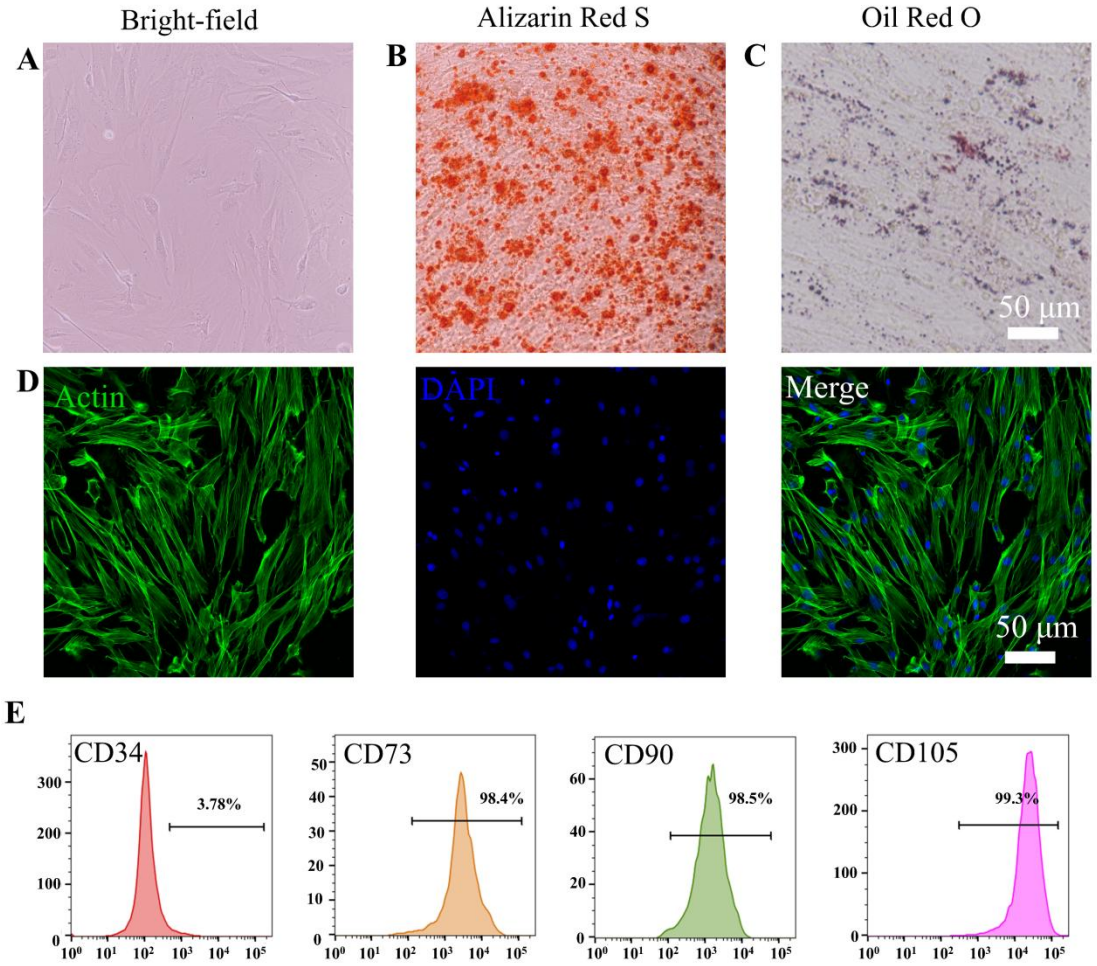


Fig 1. Multipotency and phenotypic characterization of ADSCs. (A) Bright-field morphology of P3 ADSCs. (B) Alizarin Red S staining. (C) Oil Red O staining. (D) Actin/DAPI staining. (E) Flow cytometric analysis of the expression rates of MSC surface markers CD73, CD90, CD105, and the hematopoietic stem cell marker CD34.

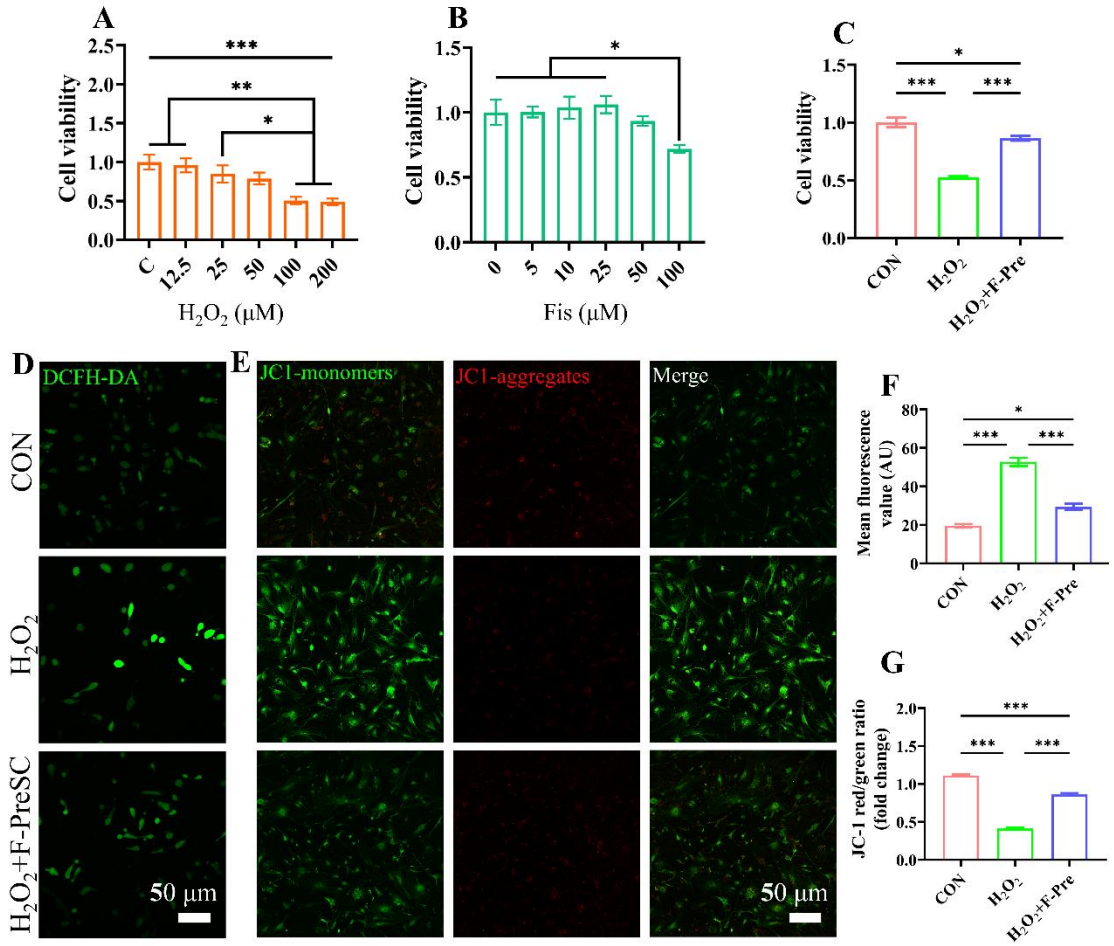


Fig 2. Fisetin pretreatment reversed H_2O_2-induced oxidative injury in ADSCs. (A) Cell viability was measured by CCK-8 assay after exposure to various concentrations of H_2O_2 for 12 h. (B) Effect of fisetin treatment for 12 h on cell viability. (C) Protective effect of 25 μM fisetin pretreatment against 100 μM H_2O_2-induced injury in ADSCs. (D) Representative fluorescence images of intracellular ROS detected by DCFH-DA probe. (E) Representative confocal images of JC-1 staining. Green fluorescence indicates JC-1 monomers (depolarized mitochondria), and red fluorescence indicates JC-1 aggregates (healthy mitochondria with intact membrane potential). (F) Quantification of ROS fluorescence intensity. (G) Quantification of the JC-1 red/green fluorescence ratio. Data are presented as mean ± SEM, n = 4 per group (*$p < 0.05$, **$p < 0.01$, ***$p < 0.001$).

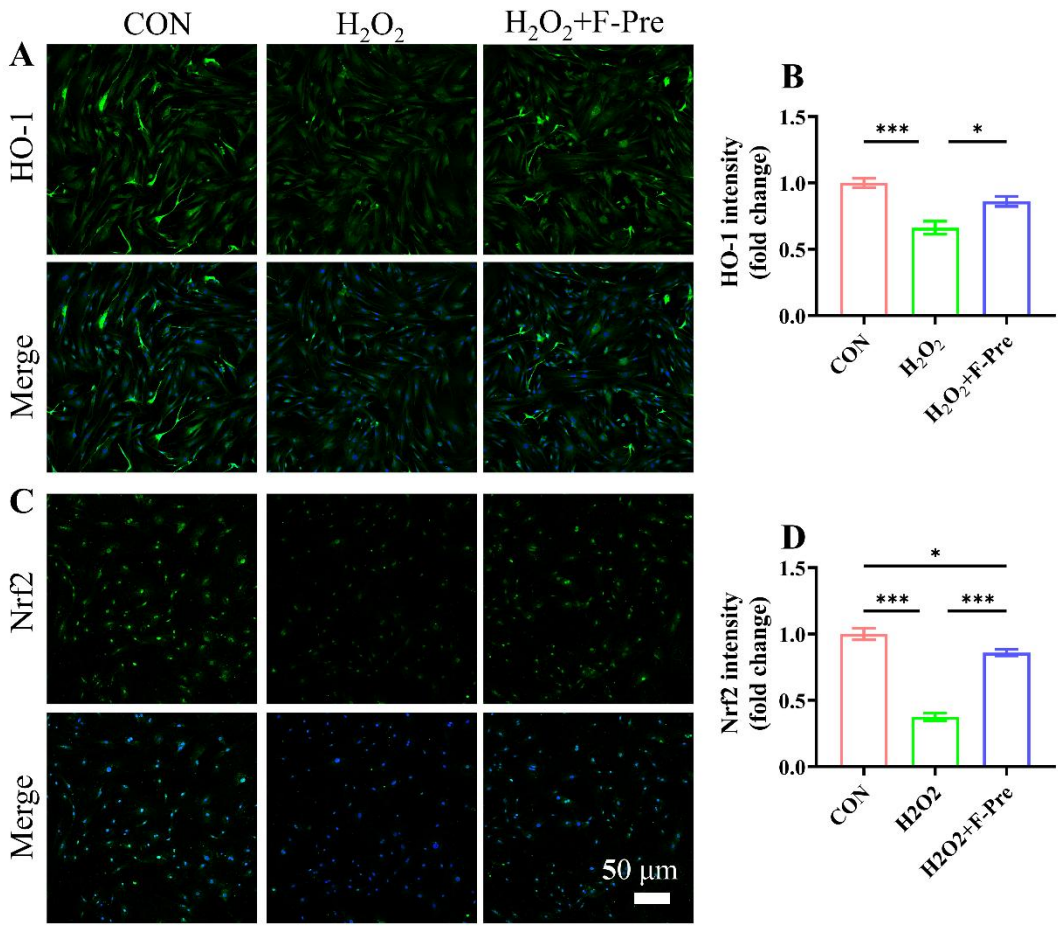


Fig 3. Fisetin upregulated endogenous HO-1 and Nrf2 expression in H_2O_2-induced ADSCs. (A) Representative immunofluorescence images of HO-1 (green) and DAPI (blue) in ADSCs. (B) Quantification of relative fluorescence intensity for HO-1. (C) Representative immunofluorescence images of Nrf2 (green) and DAPI (blue) in ADSCs. (D) Quantification of relative fluorescence intensity for Nrf2. Data are presented as mean ± SEM, n = 4 per group (*$p < 0.05$, ***$p < 0.001$).

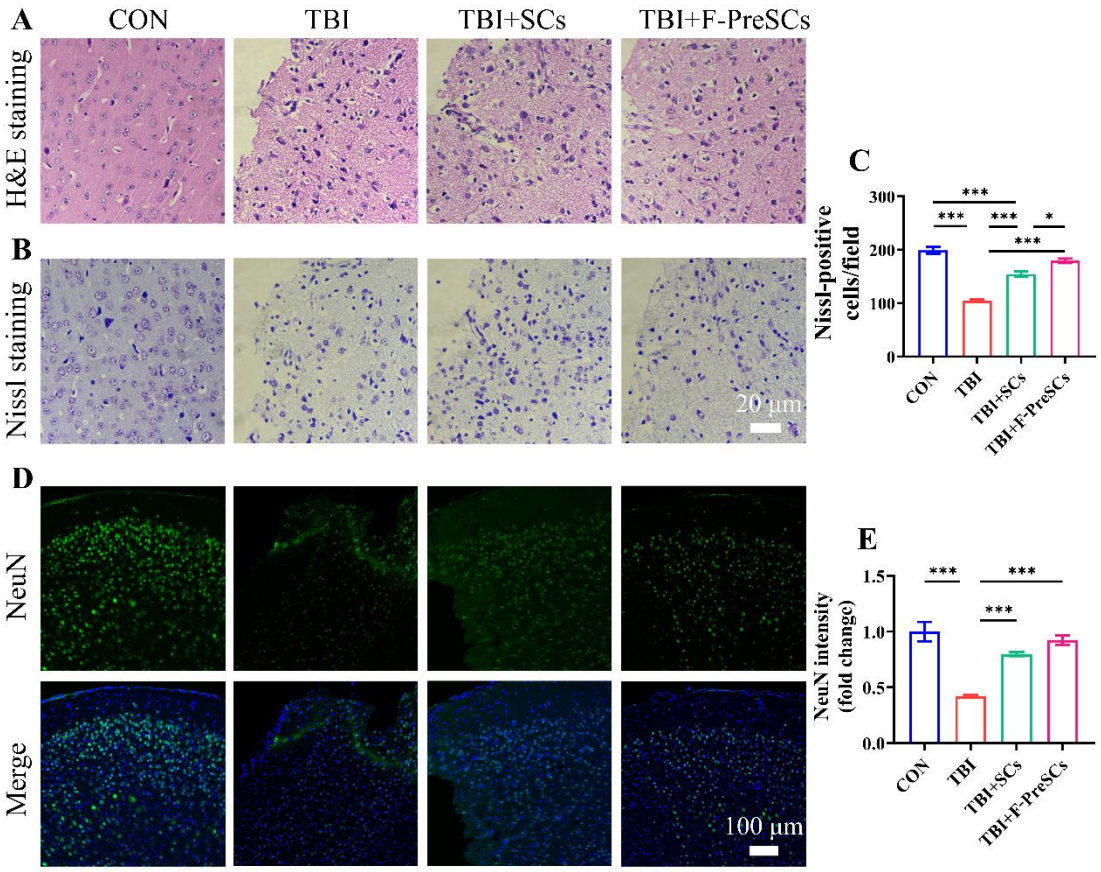


Fig 4. Intranasal transplantation of F-PreSCs reduced TBI lesions and rescued neurons. (A) H&E staining of the cerebral cortex. (B) Representative images of Nissl staining in the cerebral cortex. (C) Quantification of surviving neurons. (D) Immunofluorescence images of the mature neuronal marker NeuN in the cerebral cortex. (E) Quantification of relative fluorescence intensity for NeuN. Data are presented as mean ± SEM, n=4 per group (*$p < 0.05$, ***$p < 0.001$).

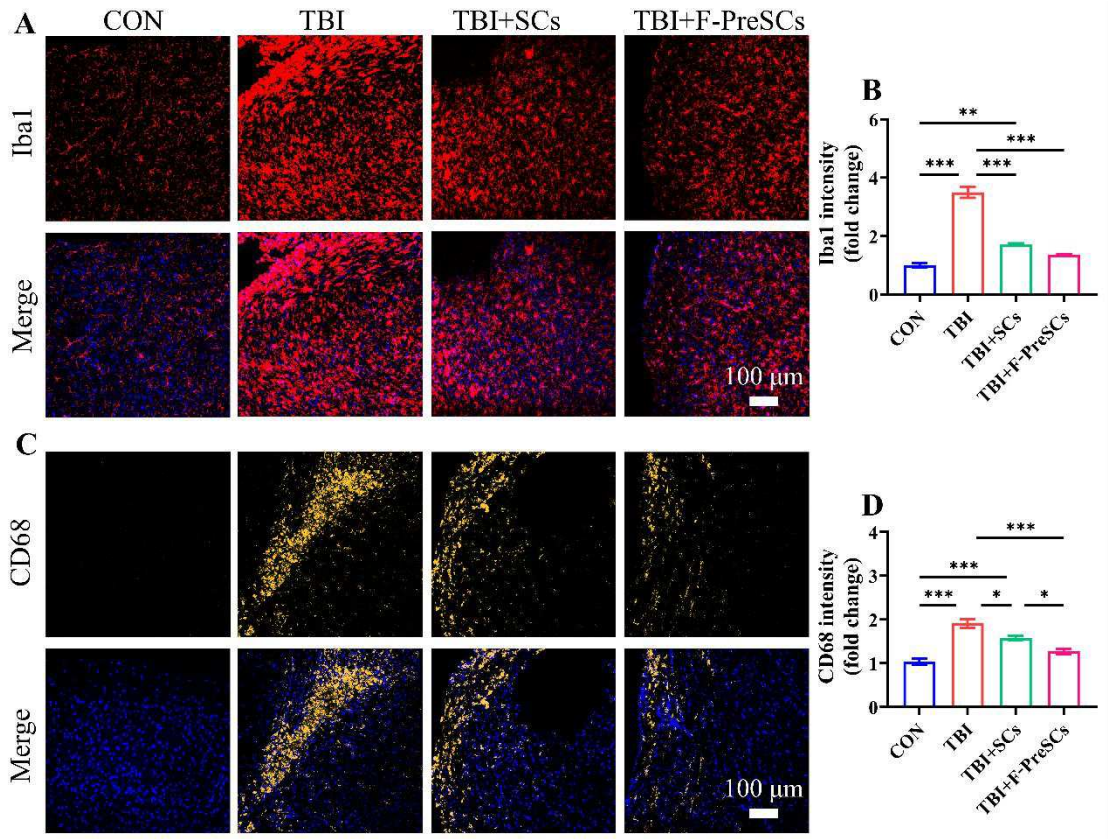


Fig 5. F-PreSCs more effectively inhibited microglial/macrophage overactivation in TBI mice. (A) Immunofluorescence images of the microglial marker Iba1. (B) Quantification of relative fluorescence intensity for Iba1. (C) Immunofluorescence images of the activated macrophage (M1-type) marker CD68. (D) Quantification of relative fluorescence intensity for CD68. Data are presented as mean ± SEM, n=4 per group (*$p < 0.05$, **$p < 0.01$, ***$p < 0.001$).

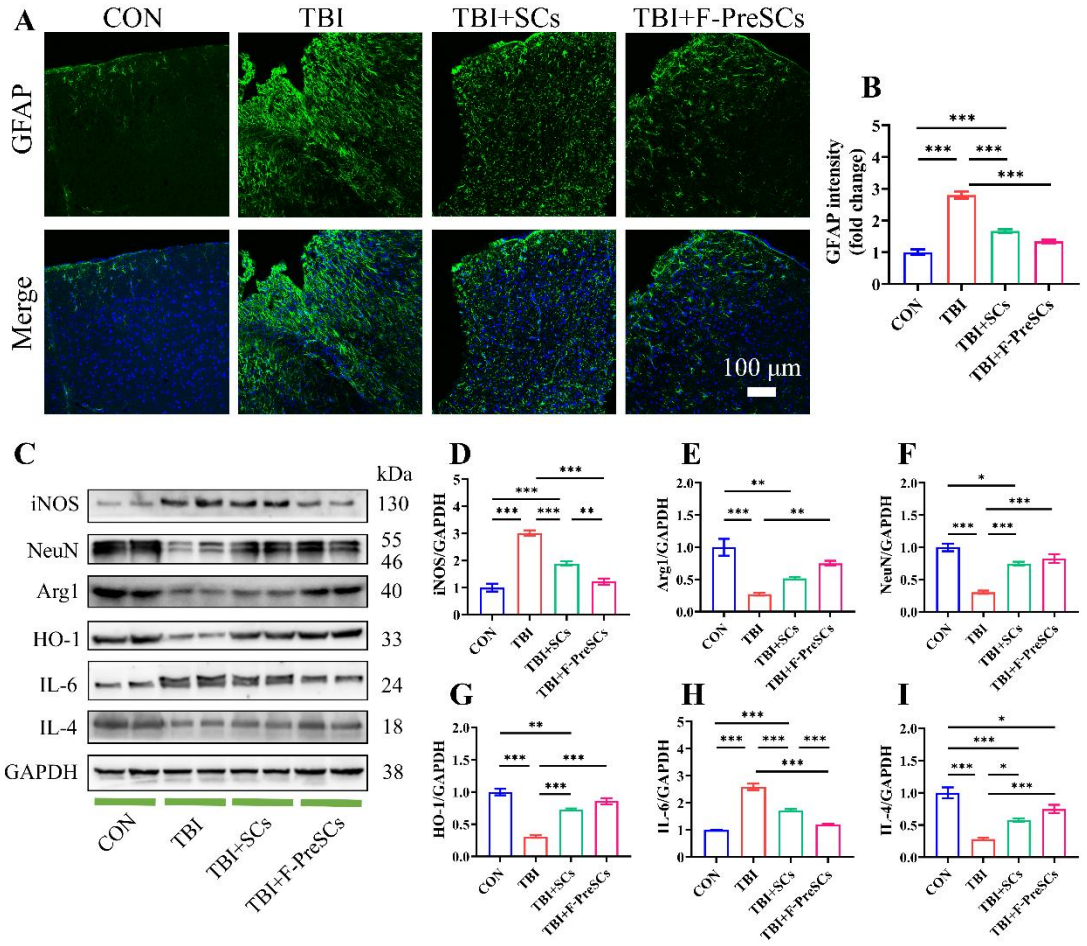


Fig 6. F-PreSCs more effectively remodeled the inflammatory and oxidative stress microenvironment. (A) Immunofluorescence images of the astrocyte marker GFAP. (B) Quantification of relative fluorescence intensity for GFAP. (C) Representative Western blot bands from ipsilateral brain tissue. (D - I) Relative protein expression levels of iNOS (D), Arg1 (E), NeuN (F), HO-1 (G), IL-6 (H), and IL-4 (I), normalized to GAPDH. Data are presented as mean ± SEM, n=4 per group (*$p < 0.05$, **$p < 0.01$, ***$p < 0.001$).

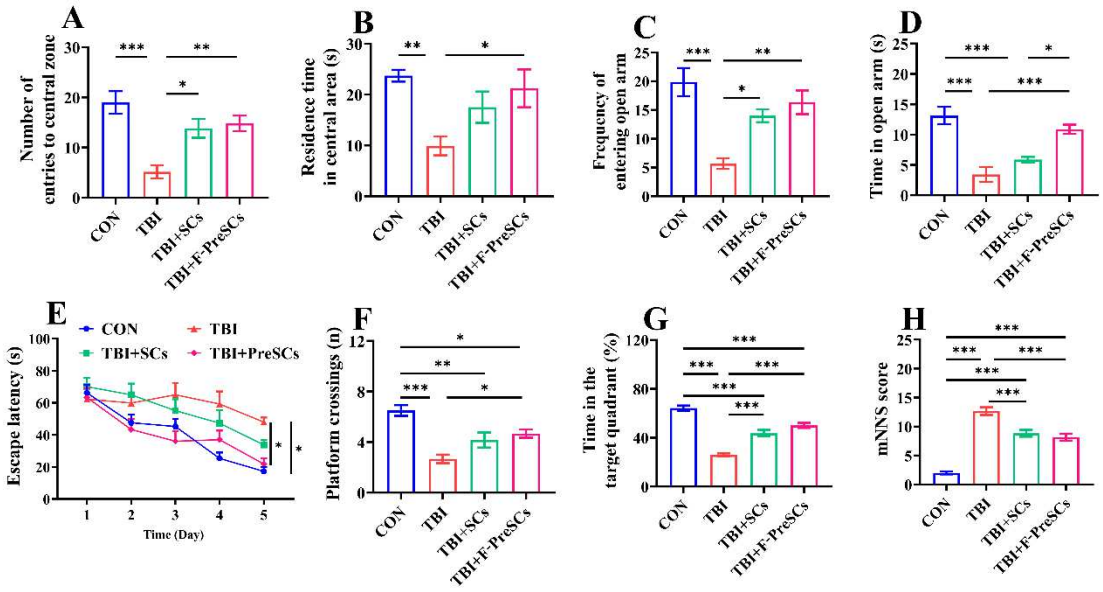


Fig 7. F-PreSCs improved sensorimotor and cognitive impairments in TBI mice. (A) Number of entries into the central zone in the OFT. (B) Residence time in the central area of the OFT. (C) Frequency of entries into the open arms in the EPM. (D) Time in the open arms in the EPM. (E) Escape latency over five consecutive days in the MWM. (F) Number of platform crossings. (G) Percentage of time in the target quadrant. (H) mNSS scores. Data are presented as mean ± SEM, n=12 per group (*$p < 0.05$, **$p < 0.01$, ***$p < 0.001$).

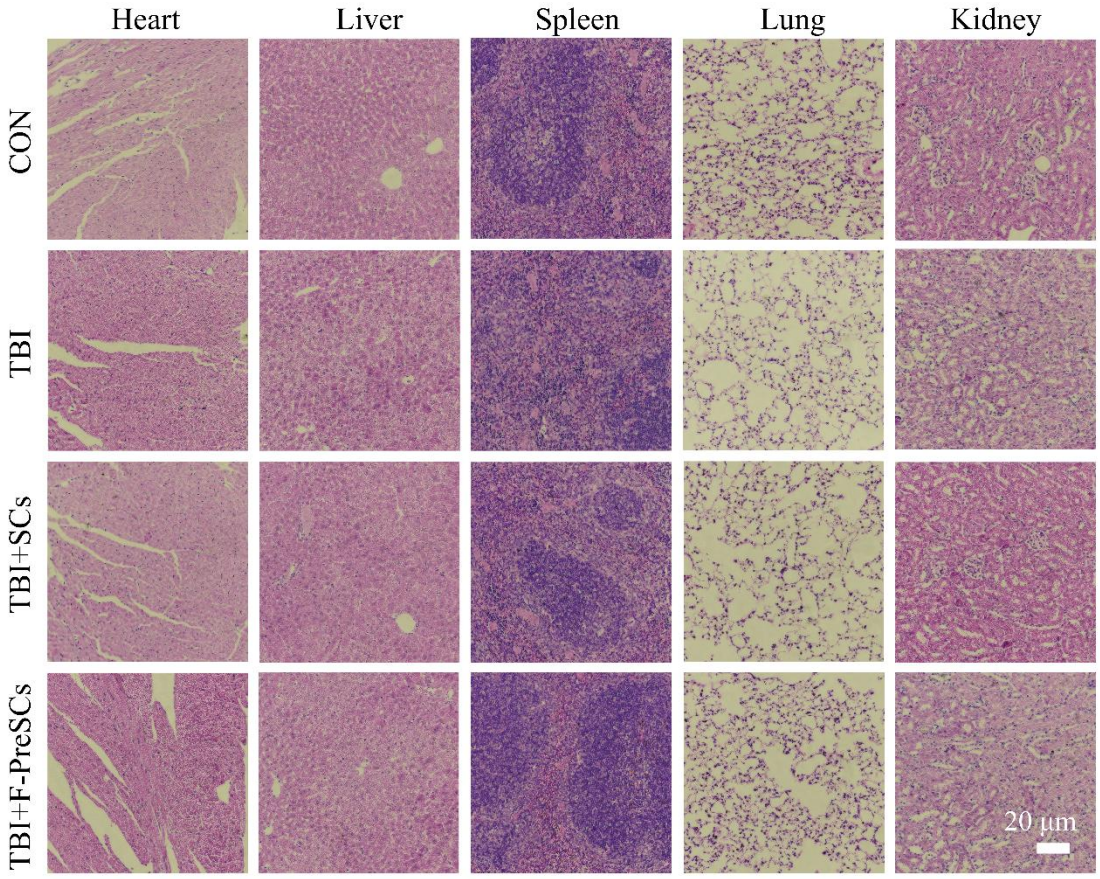


Fig 8. *In vivo* biosafety assessment of F-PreSCs transplantation. Representative H&E staining images of heart, liver, spleen, lung, and kidney from each experimental group (CON, TBI, TBI+SCs, and TBI+F-PreSCs). No overt histopathological abnormalities, inflammatory infiltration, or tissue damage were observed in any of the examined organs across all groups.

Supplementary Files

This is a list of supplementary files associated with this preprint. Click to download.

- Table1.xlsx